RSC Advances

PAPER

View Article Online
View Journal | View Issue

Cite this: *RSC Adv.*, 2017, **7**, 11041

Preparation of SiO_2/PS superhydrophobic fibers with bionic controllable micro–nano structure *via* centrifugal spinning

Yongqiang Li,*[ab] Chao Zou,[a] Jianzhong Shao,[ab] Xiangwu Zhang[c] and Ya'nan Li[a]

Received 25th October 2016
Accepted 30th January 2017

DOI: 10.1039/c6ra25813a

rsc.li/rsc-advances

The preparation of superhydrophobic micro/nano fibers has been mainly focused on the use of electrospinning; however, practical applications are limited due to cost, scale and controllable research. Herein, we present a novel and simple centrifugal spinning technology that extrudes fibers from polymer solutions by using a high-speed rotary, perforated spinneret. By controlling the concentration of the spinning solutions and adjusting the spinning parameters, polystyrene (PS) fibers with different structures have been prepared. Since PS is a low surface energy material, the surface roughness can further increase the hydrophobicity of the fibers. We prepared hydrophobic SiO_2 in different sizes, mixed them with PS dissolved in DMF, and SiO_2/PS fibers were obtained by centrifugal spinning, where the maximum water contact angle of SiO_2/PS fibers was 151° with superhydrophobicity. The typical surface of the silver ragwort leaf fibers with numerous grooves, and the lotus leaf with nano-protrusions, were successfully imitated on the centrifugally-spun SiO_2/PS fiber surface. The as-prepared PS fibers were characterized by scanning electron microscopy and water contact angle/sliding angle measurements, and a processing–structure–performance relationship was established. Results demonstrate that the fiber morphology can be easily manipulated by controlling the spinning parameters, and centrifugal spinning is a promising approach for meeting the growing demand for the mass production of superhydrophobic micro/nano fibers.

Introduction

As one of the most important aspects of surface chemistry, the wetting behavior of a liquid on a solid surface has a wide range of applications in agriculture, industry and daily life.[1] Superhydrophobic surfaces are non-wettable surfaces with a water contact angle of close to, or higher than, 150° and a sliding angle smaller than 10°.[2–4] First observed by Ollivier in 1907, superhydrophobic surfaces have gained significant attention in the past two decades, triggered by the discovery of the "lotus effect", which originates from mimicking the lotus leaves and forces water and oil drops to roll off, leaving little to no residue or trace of surface contamination.[5] The self-cleaning and anti-contamination characteristics of superhydrophobic surfaces have attracted extensive interest and they are ideal candidates for industrial applications including non-viscous coating for power lines and antennas, self-cleaning coatings for automobiles and so on.[6]

Generally, low-surface-energy materials and micrometer- or nanometer-order rough surfaces are two keys to the preparation of superhydrophobic surfaces,[4,6] based on which, many approaches have been adopted to obtain superhydrophobic surfaces, including solution-immersion, the sol–gel method, chemical vapor deposition, phase separation, the hydrothermal method, self-assembly, electrospinning, *etc.*[4,6] However, these methods are complex and time-consuming, which limit their practical applications in producing superhydrophobic surfaces. Among the variety of methods, electrospinning has been identified as one of the most versatile routes for fabricating fibers with diameters down to the nanometer scale, by utilizing high voltage on polymer solutions or melts. The electrospinning technique is capable of producing fine fibers from a variety of materials including polymers, metals and ceramics, and is able to control fiber size, composition and morphology through the adjustment of spinning solutions and conditions. In addition, electrospun nanofibers exhibit enormous surface-to-volume ratio, high porosity, small pore size, and mechanical robustness, making them promising candidates for preparing superhydrophobic surfaces.

Although the electrospinning technique offers a versatile and effective option for fabricating superhydrophobic nanofibers

[a]*Engineering Research Center for Eco-Dyeing & Finishing of Textiles, Ministry of Education, Zhejiang Sci-Tech University, Hangzhou 310018, China. E-mail: yqqli@163.com*

[b]*National and Local Joint Engineering Laboratory for Textile Fiber Materials and Processing Technology, Zhejiang Sci-Tech University, Hangzhou 310018, China*

[c]*Fiber and Polymer Science Program, Department of Textile Engineering, Chemistry and Science, North Carolina State University, Raleigh, North Carolina 27695-8301, USA*

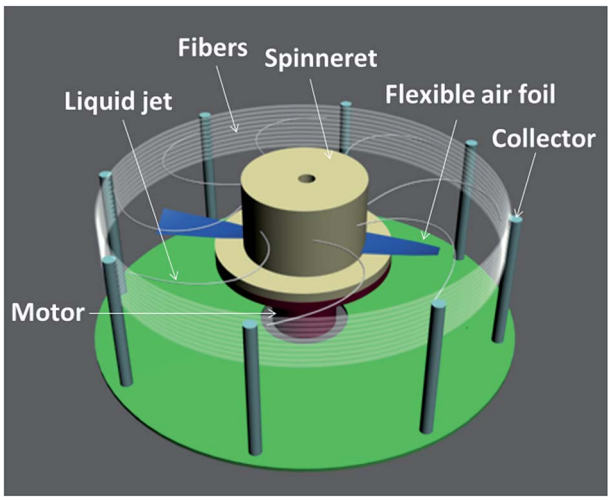

Fig. 1 Schematic of centrifugal spinning apparatus.

with controllable compositions and structures, this technique suffers from low production rate[7,8] and therefore, it cannot be the ideal solution for producing superhydrophobic fibers in a large-scale and low-cost fashion. Moreover, the application of high voltage and large amounts of solvent can potentially result in increased production costs and safety concerns. Hence, the technological impact of developing a novel nanofiber production method that can eliminate the limitations encountered by electrospinning would be significant, especially for massive production of nano-sized superhydrophobic surfaces.

Recently, several groups have demonstrated the successful fabrication of nanofibers *via* a centrifugal spinning process from a wide range of polymers,[9–13] ceramics,[14,15] and composite materials.[16–18] Compared to traditional micro–nano fiber production methods, the centrifugal spinning process has several advantages: the apparatus is simple to implement, no electric field is needed, fiber formation is independent of solution conductivity, the technology can operate with high-concentration solutions, the production rate is high and the cost is apparently low. In this work, a centrifugal spinning system has been established to promote the large-scale and low-cost production of micro–nano fibers. A schematic of the centrifugal spinning apparatus is shown in Fig. 1; it consists of a spinneret, which is located in the center of the spinning platform and contains eight small nozzles, a DC motor to rotate the spinneret, a speed controller for adjusting the rotational speed of the spinneret, eight rod collectors radially positioned in the outer perimeter, and two flexible air foils symmetrically placed below the spinneret to generate air turbulence and accommodate the fiber collection. This centrifugal spinning system is simple and is capable of eliminating the limitations of the electrospinning process.

During centrifugal spinning, a polymer solution is fed into the spinneret, which is rotated at high speed. When the rotational speed reaches a critical value, the centrifugal force overcomes the surface tension of the solution and ejects a liquid jet from each nozzle. The jet then undergoes a stretching process, accompanied by rapid solvent evaporation, and is eventually deposited on the rod collectors forming dried fibers. Using this technique, the production rate of nanofibers can be improved by at least two orders of magnitude, compared to that of the electrospinning.[8] Currently, most of the studies related to centrifugal spinning focus on the fabrication of micro–nano fibers from different materials. In the proposed work, we focus on the innovative application of this facile technique in the preparation of superhydrophobic fibers from materials such as polystyrene. The processing–structure–performance correlation is established by varying the spinning parameters and evaluating the structure and hydrophobicity of the as-prepared fibers. It is demonstrated that centrifugal spinning is a promising approach that can meet the growing demand for the mass production of superhydrophobic micro/nano fibers.

Experimental

Controllable fabrication of PS fibers

PS (M_w = 260 000 g mol^{-1}, J&K SCIENTIFIC LTD. Shanghai, China) was dissolved in DMF (Hangzhou Gaojing Fine Chemical Co. Ltd. Zhejiang, China) with stirring using a magnetic stirrer (RCT basic, IKA Works Guangzhou) for 24 hours at 60 °C, and PS solutions of 16 wt%, 18 wt%, 20 wt%, 22 wt% and 24 wt% were prepared. The rotational speed of the motor was varied from 5000 to 8000 rpm. Teflon spinnerets with different nozzle diameters (0.4 mm, 0.5 mm, and 0.6 mm) were used. The distance between the nozzle tip and the rod collector was adjustable from 6 cm to 12 cm. PS fibers with controlled morphologies were fabricated by selectively adjusting the polymer solution concentration, rotational speed, nozzle diameter, and nozzle-collector distance. All the spinning operations were conducted at room temperature.

Preparation of hydrophobic SiO_2

Different particle sizes of hydrophobic SiO_2 were prepared by the sol–gel method.[19,20] Firstly, 8 mL of deionized water (Lab-made), 120 mL of ethanol (Hangzhou Gaojing Fine Chemical Co. Ltd. Zhejiang, China) and 6.7 mL of TEOS (Tianjin Kermel Chemical Reagent Co. Ltd. Tianjin, China) were evenly mixed in a three-necked flask at 25 °C, then various amounts of ammonia (Hangzhou Gaojing Fine Chemical Co. Ltd. Zhejiang, China) were added to obtain SiO_2 sol of different particle sizes, then 3-(trimethoxysilyl)propylmethacrylate (MPS) (Aladdin Industrial Corporation. Shanghai, China) was added for 24 h to modify the SiO_2 sol, and the hydrophobic SiO_2 powder was prepared by centrifuging the sol.

Fabrication of SiO_2/PS fibers

Polystyrene is a low surface energy material, so we can improve its hydrophobicity by increasing the surface roughness. Thus, SiO_2/PS fibers were prepared by centrifugally spinning the mixture of PS, SiO_2 powder, and DMF. The SiO_2 particles introduced on the fiber surface can construct a micro–nano-rough structure and improve the hydrophobicity. In this work, SiO_2 with different particle sizes and amounts (3 wt%, 6 wt%, 9 wt%, relevant to the solution weight) together with PS were dissolved in DMF, respectively, and the mixture was stirred at

60 °C until the solution became clear. Consequently, SiO_2/PS fibers with different structures were obtained by spinning centrifugally with constant spinning parameters.

Characterization

SEM observation. The micrographs of centrifugally-spun fibers obtained using a field emission scanning electron microscope (FE-SEM, Ultra 55, Zeiss, Germany), with accelerating voltage of 1 kV. Before SEM observation, all samples were coated with gold, using a sputter coater, to reduce charge. The diameter distributions of the fibers were analyzed by combining SEM images with Nano Measurer 1.2 software, and 50 fibers were measured per sample. The mean diameters were calculated as follows:[21]

$$\overline{D} = \frac{\sum_{i=1}^{N} D_i}{N} \quad (1)$$

where $\bar{D}$ represents the average diameter of the sample, N the number of fibers, and N_i the number of fibers with diameter D_i.

Particle size measurement. The particle size of silica sol was tested using nano particle size and molecular weight analyzer (zetasizer Nano S-type, Malvern Instruments Ltd, Britain). The SiO_2 sol diluted with deionized water was measured 4 times; each time was 12 s and the mean value was taken.

FTIR measurement. The variation of the functional groups before and after modification was monitored using Fourier infrared spectroscopy (FTIR, Vertex 70, Bruker Company, Germany). The spectra were recorded in the range of 4000–500 cm^{-1}.

WCA measurement. The hydrophobicity was evaluated by measuring the contact angle of samples (DSA 20, Krüss, Germany) at ambient temperature. The volume of water droplets was 5 μL. The water contact angle of the samples was determined along with the average value of five different positions.

N_2 adsorption–desorption measurement. Nitrogen adsorption–desorption isotherms were measured on a Micromeritics ASAP 2020. The Brunauer–Emmett–Teller (BET) methods were used to analyze the specific surface areas of the samples.

Results and discussion

Controllable fabrication of PS fibers

Effect of spinning parameters on PS fibers morphology

Effect of solution concentration. To understand the correlation between concentration and fiber morphology, PS fibers from different solution concentrations were centrifugally-spun at constant operational conditions. SEM images and fiber diameter distributions are shown in Fig. 2. It can be seen that the fiber diameters increase with increasing concentration; the average fiber diameters of PS fibers centrifugally-spun from 16 wt% to 24 wt% correspond to 2 μm, 5.5 μm, 7.1 μm, 9.2 μm and 11.5 μm, respectively. In Fig. 2(a), (c) and (e), both fibers and beads are formed and the amount of fibers is small, which is due to the viscosity not being enough to make the jet stable in the spinning process. In Fig. 2(g) and (i), there are more formed fibers and fewer beads. This indicates that the jet is stabilized and forms uniform and continuous fibers, resulting from the significant increase in viscosity as the concentration increases. However, highly-viscous solutions tend to exhibit longer stress relaxation times, which limit the evaporation of the solvents and resist jet fracturing, elongation and thinning, eventually forming fibers with larger diameters. When the concentration is lower than 16 wt%, or higher than 24 wt%, no fibers are formed. This is because surface tension dominates and viscosity is low at lower concentration, while a high concentration with high viscosity would cause the nozzle to clog.

Effect of rotational speed. Centrifugal spinning is the process of utilizing centrifugal force to overcome the surface tension of polymer solutions. Centrifugal force was calculated as follows:

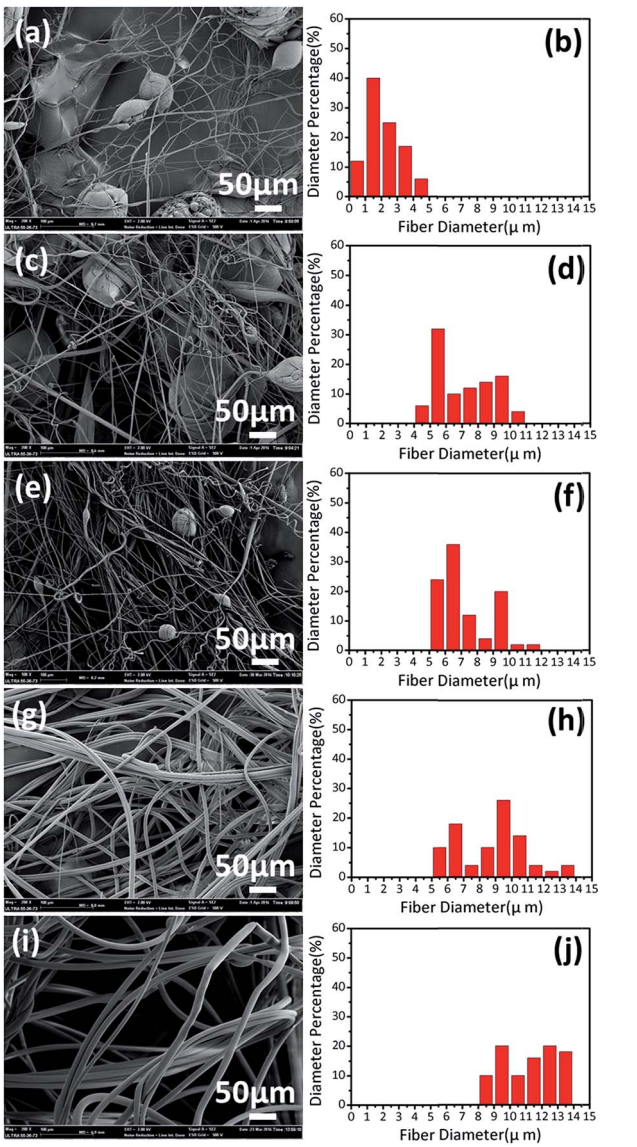

Fig. 2 SEM images and fiber diameter distributions of PS fibers centrifugally-spun at 8000 rpm using a 0.4 mm nozzle and a 12 cm nozzle-collector distance with different solution concentrations: (a and b) 16 wt%, (c and d) 18 wt%, (e and f) 20 wt%, (g and h) 22 wt%, and (i and j) 24 wt%.

$$F = m\omega^2 r \quad (2)$$

where F represents centrifugal force, m the mass of liquid jet, ω the rotational speed, r the radius of the spinneret. The values of m and r are constant, so the centrifugal force experienced by the liquid jets increases with increasing rotational speed. 16 wt% PS solution was centrifugally spun into fibers by using different rotational speeds to establish the correlation between fiber morphology and rotational speed. SEM images and fiber diameter distributions are shown in Fig. 3, where the average fiber diameters are 9 μm, 5.5 μm, 3.3 μm and 2 μm, prepared at rotational speeds from 5000 to 8000 rpm, respectively. This is because a higher centrifugal force can induce greater extension and thinning of polymer jets, which in turn results in finer fibers.

Effect of nozzle diameter. The nozzle diameter can control the mass throughput of the liquid jet. An increase in nozzle diameter creates larger mass throughput, which in turn accelerates the fiber diameter. In this work, the effect of the nozzle diameter on fiber morphology was studied by using three spinnerets with nozzle diameters of 0.4, 0.5, and 0.6 mm. SEM images and fiber diameter distributions are shown in Fig. 4. The average fiber diameter increased from 2 μm to 3.2 μm to 4 μm as the nozzle diameter increased.

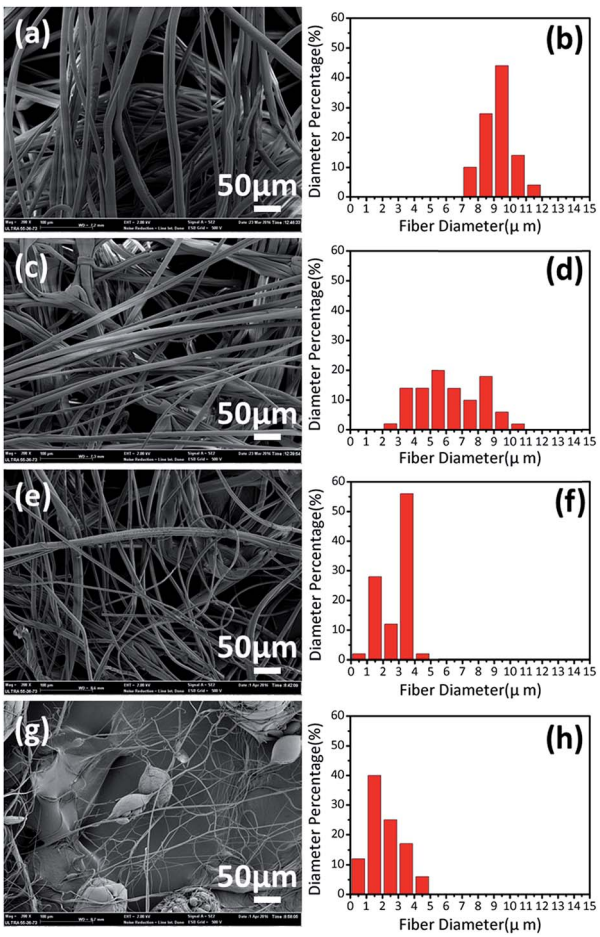

Fig. 3 SEM images and fiber diameter distributions of PS fibers centrifugally-spun from a 16 wt% solution using a 0.4 mm nozzle and a 12 cm nozzle-collector distance at different rotational speeds: (a and b) 5000 rpm, (c and d) 6000 rpm, and (e and f) 7000 rpm, (g and h) 8000 rpm.

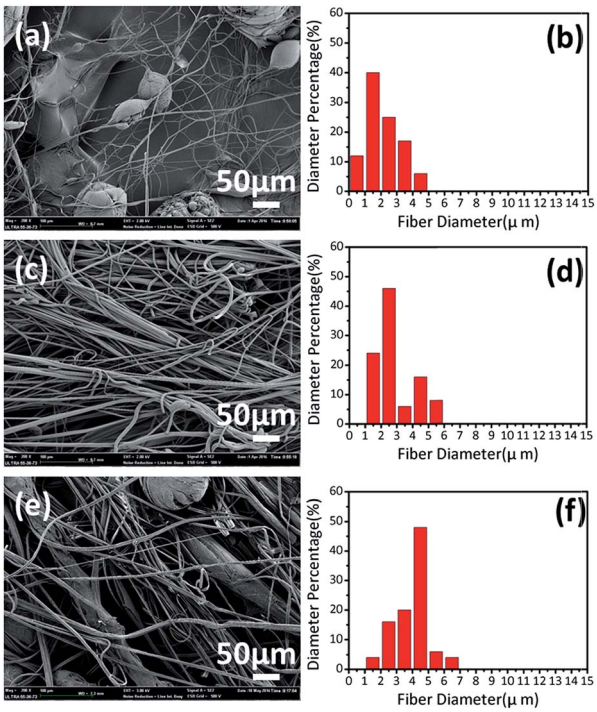

Fig. 4 SEM images and fiber diameter distributions of PS fibers centrifugally-spun from a 16 wt% solution at 8000 rpm using a 12 cm nozzle-collector distance with different nozzle diameters: (a and b) 0.4 mm, (c and d) 0.5 mm, and (e and f) 0.6 mm.

Effect of nozzle-collector distance. The fiber morphology is also closely related to the evaporation rate of the solvent in the centrifugal spinning process. Thus, varying the nozzle-collector distance can affect the evaporation rate of the solvent by changing the flight time of the liquid jet; the longer nozzle-collector distance means the liquid jet can have a longer distance to travel, which may favor the formation of finer fibers. The relationship between fiber morphology and nozzle-collector distance was studied by varying the nozzle-collector distance from 6 to 12 cm. SEM images and fiber diameter distributions are shown in Fig. 5. The average fiber diameters were 2.5, 2.3 and 2 μm, corresponding to 6, 9 and 12 cm of nozzle-collector distances, respectively.

For preparing uniform fibers, the optimized conditions of solution concentration should be higher than 20 wt%, with the highest rotational speed, the smallest nozzle diameter and the longest nozzle-collector distance, on the basis of the test above. The relationship between fiber diameter and the parameters is as follows:[22]

$$D \sim \frac{a}{R_c^{3/2} n} \quad (3)$$

where D represents fiber diameter, a the nozzle diameter, R_c the nozzle-collector distance, n the rotational speed.

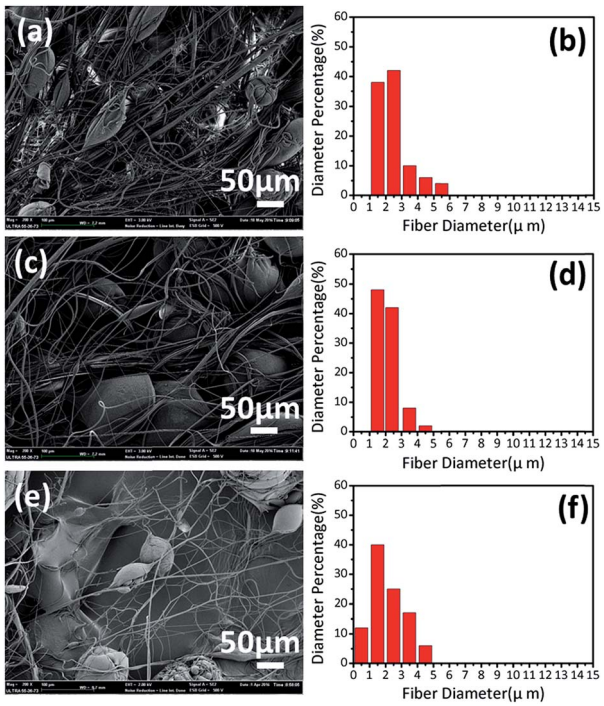

Fig. 5 SEM images and fiber diameter distributions of PS fibers centrifugally-spun from the 16 wt% solution at 8000 rpm using a nozzle with 0.4 mm diameter and different nozzle-collector distances: (a and b) 6 cm, (c and d) 9 cm, and (e and f) 12 cm.

Topography of centrifugal-spun PS fibers

PS fibers centrifugally-spun at 8000 rpm using a 0.4 mm nozzle and 12 cm nozzle-collector distance with different solution concentrations generally have the following four kinds of surface topography, as shown in Fig. 6: (a) porous surface, (b) grooved surface, (c) wrinkled surface, (d) smooth surface. The surface topology of PS fibers prepared from low and high solution concentrations are displayed in Fig. 6(a) and (c), respectively; between the two concentrations corresponds mostly to Fig. 6(b), and the smooth surface structure in Fig. 6(d) slightly exists in PS fibers prepared from each solution concentration. The interpretation of the structure in Fig. 6(a) is that the regular phase morphology is generated by rapid phase separation during the centrifugal spinning process. Polymer rich regions are quickly cured to form a substrate and the solvent rich regions are apparently transformed into pores. When the fluid jet is ejected into the surroundings, a glassy shell is formed on the surface of the fluid jet due to solvent evaporation and simultaneously, the solvent trapped inside diffuses out from the core to the surface. Thus, a contraction mismatch between core and shell occurs, resulting in the formation of wrinkled surfaces[23] in Fig. 6(c). The intermediate state between pore and wrinkle is the groove, shown in Fig. 6(b).

Results show that the morphology of the PS fibers can be easily manipulated by selectively controlling the spinning parameters, and the typically rough surface of the silver ragwort leaf fibers with nano-scaled grooves was successfully imitated by creating wrinkles on the PS fibers surface (Fig. 6(c)).

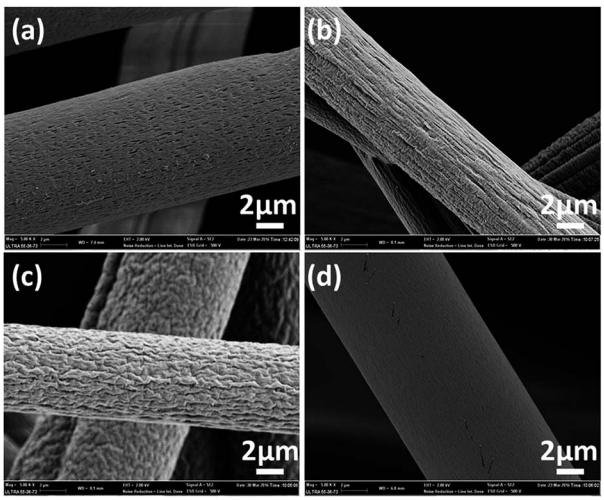

Fig. 6 SEM images of PS fibers with different surface topologies centrifugally-spun at 8000 rpm using 0.4 mm nozzle diameter and 12 cm nozzle-collector distances with different solution concentrations.

Preparation of hydrophobic SiO_2

In this study, hydrophobic SiO_2 was prepared by the sol–gel method; the particle sizes were 122 nm, 210 nm and 306 nm, respectively. FTIR-ATR spectra of SiO_2 before and after modification are shown in Fig. 7. The spectrum of the modified SiO_2 particles shows a weak carbonyl (C=O) stretching vibration peak at 1720 cm^{-1}, which indicates that MPS has been grafted onto SiO_2 particles; the characteristic peaks at 1460 cm^{-1} and 2960 cm^{-1} belong to CH_x.

Fabrication of SiO_2/PS micro/nano fibers

Scanning electron microscopy was used to observe the surface topography of PS fibers after their introduction onto SiO_2. SEM images of SiO_2/PS fibers are shown in Fig. 8, where it can be

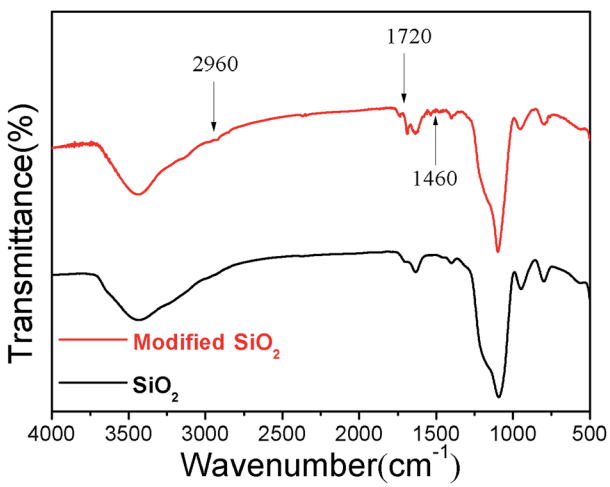

Fig. 7 FTIR-ATR spectra of SiO_2 before and after modification.

seen that the SiO_2 particles are randomly distributed until they cover the fiber surface. The surface roughness of SiO_2/PS fibers is increased because of the presence of SiO_2 on the surface, but some of the SiO_2 particles are dispersed in pores, grooves and wrinkles, thus reducing the surface roughness. As such, the fiber surface gradually becomes smooth with increasing SiO_2 content, and different SiO_2 sizes also have influence on the fiber surface structure. As particle size increases, pores on the fiber surface gradually turn into grooves and then wrinkles, probably because the evaporation rate of the solvent decreases during fiber formation.

Hydrophobicity of PS fibers

In order to investigate the hydrophobicity of PS fibers, we measured the water contact angles; the results are shown in Fig. 9. The water contact angle of PS fibers decreases with increasing PS concentration, because PS fibers centrifugally-spun from lower solution concentration have smaller diameters and bead structures, giving larger surface roughness and resulting in higher hydrophobicity. In the case of SiO_2/PS fibers, the PS fibers with 3 wt% of SiO_2 have a maximum water contact angle of 151°. Although less SiO_2 particles are attached to the fiber surfaces, there are more pores, grooves and wrinkles, thus resulting in larger surface roughness as a whole. PS fibers with 6 wt% SiO_2 content have the minimum water contact angle. SiO_2 particles on the fiber surfaces increase, but pores, grooves and wrinkles are smaller and less. Simultaneously, the fiber surfaces tend to be flat due to the presence of some SiO_2 in pores, grooves and wrinkles. PS fibers with 9 wt% SiO_2 content are in the middle, a large number of SiO_2 particles covered the fiber surface creating a greater increase in surface roughness. According to the Cassie–Baxter model,[24] if the unevenness of the solid surface roughness causes macro fluctuation to a certain degree, there will be more air stored in the recessed portion when the surface comes in contact with liquid. In this case, the apparent surface area of the complex surface consists of solids and gaseous substances. High roughness reduces the fraction of the fiber surface, while the air portion increases, resulting in a decrease in the area of the fiber surface in contact with the droplet and improvement in the hydrophobicity.

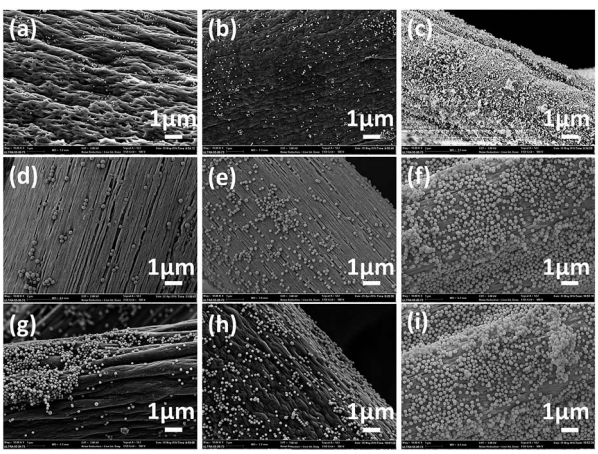

Fig. 8 SEM images of SiO_2/PS fibers centrifugally-spun from 16 wt% solution at 8000 rpm using nozzle diameter of 0.4 mm and nozzle-collector distance of 12 cm with different SiO_2 particle sizes: (a)–(c) 122 nm; (d)–(f) 210 nm; (g)–(i) 306 nm; and concentrations: (a), (d) and (g) 3 wt%, (b), (e) and (f) 6 wt%, (c), (f) and (i) 9 wt%.

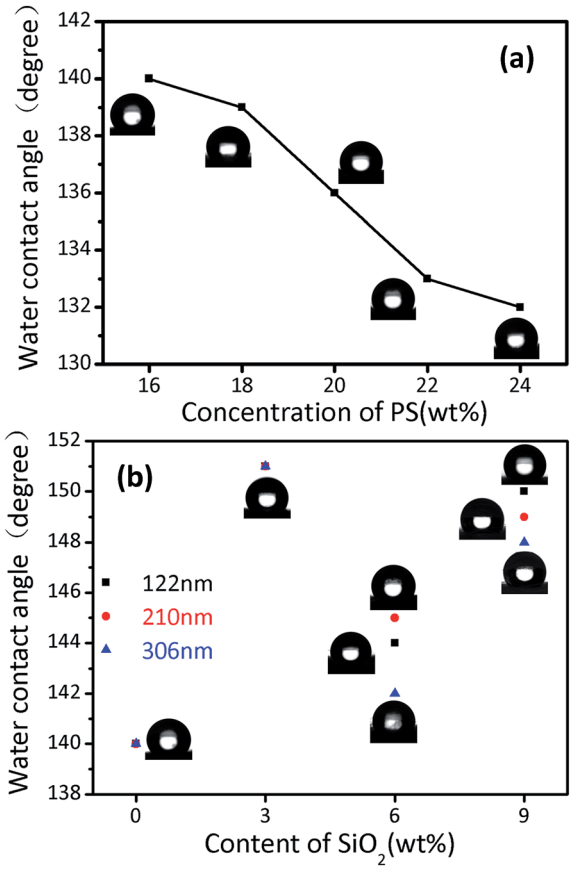

Fig. 9 WCA and the corresponding shapes of water droplets for the PS fibers centrifugally-spun from (a) different PS solution concentrations and (b) 16 wt% solution at 8000 rpm using a nozzle with diameter of 0.4 mm and nozzle-collector distance of 12 cm, with different particle size and SiO_2 content.

The typically hydrophobic surface of the silver ragwort leaf fibers with numerous grooves and the lotus leaf with nano-protrusions were successfully imitated in the SiO_2/PS fibers surface, shown in Fig. 8(g). This indicates that the dual-biomimetic, superhydrophobic fibers can be centrifugally spun from a mixed solution of PS and silica nanoparticles (Fig. 10).

N_2 adsorption–desorption measurement

The PS fiber surface was completely covered by SiO_2 when the SiO_2 content reached 9 wt%, but there was still lots of SiO_2 in the fiber, as shown in Fig. 11. It can be seen that internally, the PS fiber exhibits a fluffy, porous structure. We also used Brunauer–Emmett–Teller (BET) methods to analyze the specific surface areas of SiO_2/PS fibers.

The presence of SiO_2 in addition to the pores, grooves and wrinkles on the fiber surfaces cause SiO_2/PS fibers to have

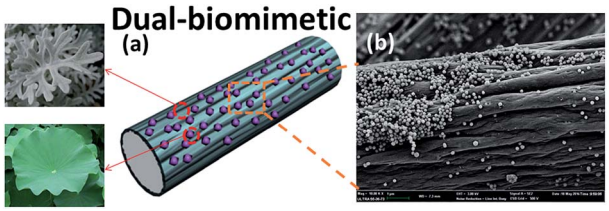

Fig. 10 Dual-biomimetic superhydrophobic PS fibers from a combination of the ragwort leaf and lotus leaf. (a) Schematic of the biomimetic superhydrophobic surfaces. (b) SEM images of PS fibers containing 3 wt% SiO_2 nanoparticles with size of 306 nm, formed from DMF. Upper inset shows the silver ragwort leaf and the lower inset shows the lotus leaf.

a relatively higher SSA. It is shown in Fig. 12 that as the SiO_2 content increases, that the trends of fiber SSA and pore volume are almost the same, increasing first and then decreasing. When the SiO_2 content is 6 wt%, fiber SSA and pore volume are the maximum, 21.0448 m^2 g^{-1} and 0.109972 cm^3 g^{-1}, respectively.

Fig. 13 shows isotherms obtained by the nitrogen adsorption/desorption test. The shape of the curves in Fig. 13 represent adsorption/desorption isotherms of typical

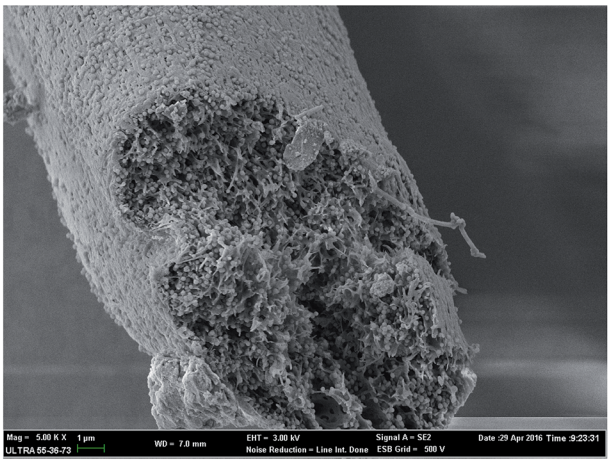

Fig. 11 SEM image of 9 wt% SiO_2/PS fiber cross-section.

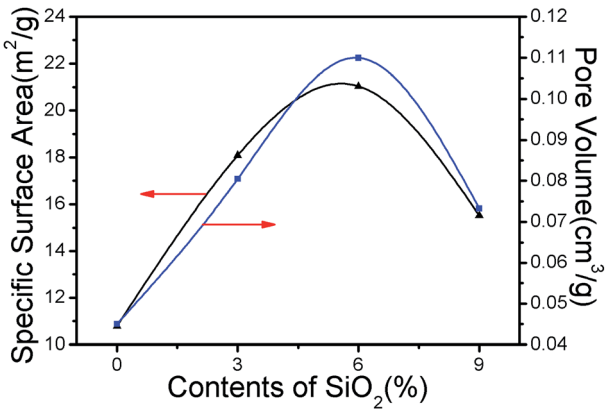

Fig. 12 Effect of SiO_2 content on SiO_2/PS fibers SSA and pore volume.

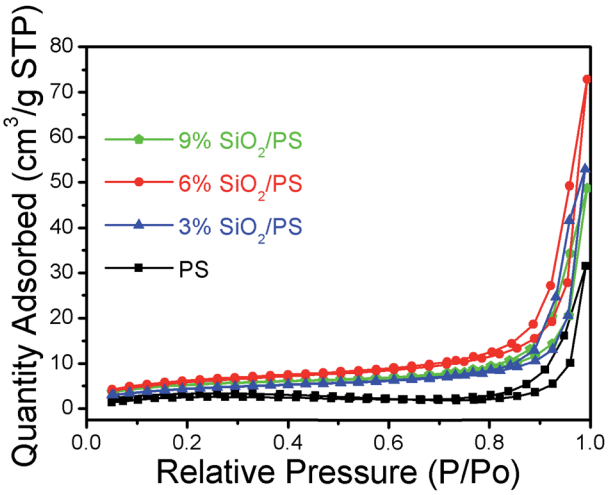

Fig. 13 Nitrogen adsorption/desorption isotherms of SiO_2/PS fibers.

mesoporous materials (Type IV),[25] and the adsorption curve falls behind the desorption curve, while the presence of the hysteresis curve confirms the presence of the porous structure. According to the isotherm classification criteria established by International Union of Pure and Applied Chemistry,[25] the hysteresis loop in this figure belongs to the H3 type, which means that pores are present in the test material, and the shape of the pore is long and filamentary.

Conclusions

A facile and effective centrifugal spinning system was developed to quickly fabricate superhydrophobic PS fibers by using a high-speed rotary spinneret. We used this technology to effectively prepare superhydrophobic PS fibers. The different parameters, such as solution concentration, the content and size of SiO_2, rotational speed, nozzle diameter and nozzle-collector distance, are related to fiber morphology. Results show that the morphology of the fibers can be easily manipulated by selectively controlling spinning parameters. The typically hydrophobic surface of the silver ragwort leaf fibers with numerous grooves, and the lotus leaf with nano-protrusions, were successfully imitated in centrifugally-spun SiO_2/PS fiber surfaces. In addition, the as-prepared SiO_2/PS fiber internally exhibits a fluffy, porous structure, which can be used for other applications as well. As a result, the centrifugal spinning technology is a promising approach for superhydrophobic fiber production in a low-cost and large-scale fashion.

Acknowledgements

This work is supported by the National Natural Science Foundation of China (No. 51403189), Financial support from the Science and Technology Department of Zhejiang Province (No. 2017C31102), Science Foundation of Zhejiang Sci-Tech University (ZSTU) (No. 13012139-Y), and Open Foundation of Zhejiang Provincial Top Key Academic Discipline (2016YXQN08).

References

1 K. Liu, X. Yao and L. Jiang, *Chem. Soc. Rev.*, 2010, **39**, 3240–3255.
2 P. Roach, N. J. Shirtcliffe and M. I. Newton, *Soft Matter*, 2008, **4**, 224–240.
3 M. Ma and R. M. Hill, *Curr. Opin. Colloid Interface Sci.*, 2006, **11**, 193–202.
4 X. L. Sheng and J. H. Zhang, *Langmuir*, 2009, **25**, 6916–6922.
5 X. Wang, B. Ding, J. Yu and M. Wang, *Nano Today*, 2011, **6**, 510–530.
6 Y. Song, L. Wang, X. Wang, K. Bian, Q. Yang and Y. Li, *J. Appl. Polym. Sci.*, 2014, **131**, 40718.
7 Y. Lu, Y. Li, S. Zhang, G. Xu, K. Fu, H. Lee and X. Zhang, *Eur. Polym. J.*, 2013, **49**, 3834–3845.
8 Z. McEachin and K. Lozano, *J. Appl. Polym. Sci.*, 2012, **126**, 473–479.
9 H. Liu, Y. Chen, S. Pei, G. Liu and J. Liu, *J. Sol-Gel Sci. Technol.*, 2013, **65**, 443–451.
10 S. Padron, R. Patlan, J. Gutierrez, N. Santos, T. Eubanks and K. Lozano, *J. Appl. Polym. Sci.*, 2012, **125**, 3610–3616.
11 M. R. Badrossamay, H. A. McIlwee, J. A. Goss and K. K. Parker, *Nano Lett.*, 2010, **10**, 2257–2261.
12 B. Vazquez, H. Vasquez and K. Lozano, *Polym. Eng. Sci.*, 2012, **52**, 2260–2265.
13 M. A. Hammami, M. Krifa and O. Harzallah, *J. Text. Inst.*, 2014, **105**, 637–647.
14 A. Altecor, Y. Mao and K. Lozano, *Funct. Mater. Lett.*, 2012, **05**, 1250020.
15 M. Yanilmaz, Y. Lu, Y. Li and X. Zhang, *J. Power Sources*, 2015, **273**, 1114–1119.
16 B. Weng, F. Xu and K. Lozano, *J. Appl. Polym. Sci.*, 2014, **131**, 40302.
17 B. Weng, F. Xu, A. Salinas and K. Lozano, *Carbon*, 2014, **75**, 217–226.
18 E. Bourgeat-Lami and J. Lang, *J. Colloid Interface Sci.*, 1998, **197**, 293–308.
19 S. W. Zhang, S.-X. Zhou, Y. M. Weng and L. M. Wu, *Langmuir*, 2005, **21**, 2124–2128.
20 D. Z. Wu, L. Z. Jiang, J. Y. Zhan and R. G. Jin, *J. Beijing Univ. Chem. Technol., Nat. Sci. Ed.*, 2007, **34**, 287–289.
21 B. Peng, E. van der Wee, A. Imhof and A. van Blaaderen, *Langmuir*, 2012, **28**, 6776–6785.
22 Z. M. Zhang, S. Q. Mei and Q. Xu, *Manuf. Autom.*, 2013, **35**, 82–87.
23 L. Wang, C.-L. Pai, M. C. Boyce and G. C. Rutledge, *Appl. Phys. Lett.*, 2009, **94**, 151916.
24 A. B. D. Cassie and S. Baxter, *Trans. Faraday Soc.*, 1944, **40**, 546–551.
25 S. J. Gregg and K. S. W. Sing, *Adsorption, surface area, and porosity*, Academic Press, 1982.